Hindawi
Advances in Materials Science and Engineering
Volume 2019, Article ID 8361095, 11 pages
https://doi.org/10.1155/2019/8361095

Research Article

Crack Resistance Properties of HPFRC Beam-Column Joints under Cyclic Load

Dehong Wang[1,2] **Yanzhong Ju**[1] **and Hao Shen**[1]

[1]*School of Civil Engineering and Architecture, Northeast Electric Power University, Jilin 132012, China*
[2]*Key Lab of Structures Dynamic Behavior and Control (Harbin Institute of Technology), Ministry of Education, Harbin 150090, China*

Correspondence should be addressed to Dehong Wang; hitwdh@126.com and Yanzhong Ju; juyanzhong@126.com

Received 26 June 2018; Accepted 3 January 2019; Published 4 March 2019

Academic Editor: Zbyšek Pavlík

To investigate the crack resistance properties of high-performance fiber-reinforced concrete (HPFRC) beam-column joints, quasi-static tests of twenty-four beam-column joint specimens were performed. Test specimen variables included joint types, size effect, axial compression ratio, stirrup ratio in joint, web reinforcement, and noncorner vertical reinforcement across the joint region. The influences of these factors on the crack properties of HPFRC joints were analyzed. Test results showed that the shear strength at the crack of HPFRC exterior joints with shear failure was closer to the ultimate bearing capacity. The average ratio of the cracking shear force to the peak shear force was 0.631 for the exterior joint with shear failure, and the ratio was 0.527 for the interior joint with the same size. The size effect was observed in HPFRC joint specimens, and the average shear stress at the joint crack decreased with the increase of the joint specimen size. The increase of the axial compression ratio can improve the crack resistance properties (cracking strength and crack width) of HPFRC joints. Web reinforcement and noncorner vertical reinforcement across the joint region have no evident influence on the cracking strength of joints, but they significantly affect the distribution and width of cracks in the joint region. The formulas for calculating the cracking strength and crack width of HPFRC joints were proposed based on the test results.

1. Introduction

Cracks appear when the strain of concrete reaches the ultimate tensile strain. The ultimate tensile strain of normal concrete is small, so it is easy to crack. The crack is one of the important influence factors for durability of the structure. Li and Melchers [1] studied the corrosion-induced crack relationship and derived an analytical model for corrosion-induced crack width based on the concept of smeared cracks. It was found that the corrosion rate was the most important factor affecting the time to surface cracking and the growth of crack width. It is extremely important to control the crack of concrete in important structures or for components to ensure the durability of reinforced concrete structures, especially in coastal regions and salt lake regions with a serious corrosive environment. In coastal regions, the climate is humid and hot, and the chloride ions in the sea penetrate in concrete in the form of sea fog and result in corrosion, which seriously affects the performance and service life of reinforced concrete structures [2]. Additionally, the durability problems of reinforced concrete structures in salt lake regions are more significant and complex than those on coastal regions [3].

Oh and Kang [4] conducted a series of tests on reinforced concrete beams and developed formulas for predicting the maximum crack width and average crack spacing in reinforced concrete flexural members. Biolzi and Cattaneo [5] conducted thirty-six steel fiber-reinforced concrete beams with and without conventional shear reinforcement and studied crack patterns and load at first cracking. The crack opening and crack spacing of the steel fiber-reinforced concrete were smaller than those without fiber. The formula

for calculating crack width of the steel fiber-reinforced concrete was presented in the paper. Silva et al. [6] studied the shear cracking behavior of prestressed reinforced concrete (PRC) beams. The results revealed that the prestressing force significantly reduced shear crack width in PRC beams compared to RC beams. Muttoni and Ruiz [7] studied the shear mechanism of beams after cracks and established an estimation model of shear strength of members without shear reinforcement. Mansur et al. [8] presented a simple method for calculating the crack width of reinforced concrete members based on the "bond theory."

At present, there are few researches on crack and crack width of the beam-column joint. Xing et al. [9] conducted a crack resistance test of interior joints with abrupt reduction in beam section in a reinforced concrete frame and put forward a formula for calculating the crack bearing capacity of beam-column joints variable section. Filiatrault et al. [10] conducted a quasi-static test of three full-scale beam-column joints. Two specimens were made of normal concrete, and one was made of steel fiber concrete; the volume content of the steel fiber was 1.6%. The results showed that the cracking load of the steel fiber concrete joints was 50% higher than that of the normal concrete joints with the same reinforcement. Thus, the use of steel fiber concrete can improve the crack resistance properties of RC members, and the high-performance fiber-reinforced concrete (HPFRC) with high cracking strain and super durability can be an effective method to solve the durability problems of reinforced concrete structures.

HPFRC is a cement-based fiber-reinforced composite material with excellent mechanical properties and durability [11, 12]. Choi et al. [13] investigated the effect of the steel fiber volume content on mechanical properties of high-performance concrete. The results indicate that there is no significant difference in compressive strength with the increase of volume fraction of steel fiber, but the tensile and flexural properties of UHPC have been greatly improved. Mo et al. [14] have conducted over 60 freeze-thaw cycle tests on ultra-high-performance concrete. The results showed that the chloride ion permeability and mass loss of UHPC can be neglected. In recent years, lot of research on the performance of HPFRC components has been done [15–17]. Al-Osta et al. [18] studied the flexural properties of normal concrete beams and HPFRC beams. And bond strength tests show that HPFRC has good bonding property, even without surface preparation of the concrete substrate. Zheng et al. [19] conducted tests of 14 reactive powder concrete beams with axial compressive strength of 102 MPa. The results indicated that the bending tensile cracking strain of the rectangular section RPC beam is 750×10^{-6} and the ultimate compressive strain is 5500×10^{-6}, far higher than the normal concrete.

The tensile strength and cracking stress of HPFRC are significantly higher than that of the normal concrete and high-strength concrete [20–22]. Thus, the performance of HPFRC components must differ from that of the normal concrete. It is very necessary to study the crack resistance properties and calculate the cracking load and crack width of HPFRC joints.

2. Experimental Programs

2.1. Description of Specimen. In the experiment, 24 HPFRC beam-column joint specimens were designed and manufactured. The test parameters include five main factors, namely, the type of joints, axial compression ratio, stirrup ratio in the joint, web reinforcement, and noncorner vertical reinforcement across the joint region amount to five influential factors. Table 1 shows the design parameters for each specimen. Specifically, there were 12 exterior joint specimens, 4 interior joint specimens with a scale of 1/2, and 8 interior joint specimens with a scale of 3/4. The column cross section of the 1/2-scale specimen was 200 mm × 200 mm and the beam cross section was 150 mm × 250 mm, and the size of the specimens was reported in references [23, 24]. The column cross section of the 3/4-scale specimen was 300 mm × 300 mm and the beam cross section was 250 mm × 350 mm. Figure 1 shows the details of the sizes and the reinforcement of the specimens. The test results of mechanical properties of steel bars are listed in Table 2. The mixture proportions of HPFRC were reported in the previous study [25].

2.2. Test Setup and Loading Procedure. In this experiment, the beam tips were subjected to quasi-static load, the column end was subjected to a constant load, and the top of the column and the bottom of the column were hinged supports. The test loading diagram is shown in Figure 2. The top load of the column was applied via a 2000 kN hydraulic jack, and the load sensor was arranged below the jack to measure the load during the test and maintain a constant axial pressure. The reciprocating load of beam end was applied by an electrohydraulic servo actuator. In terms of Chinese codes [26], the test loading system of the test adopts the loading system controlled via a mix of load and displacement control. In other words, the loading process consisted of two stages. Load control was adopted at the initial stage of loading, and each load level was recycled once. When cracking occurs to the joint region of the specimens or the longitudinal reinforcements in the beam reached the yield strain, the displacement control was used as opposed to the load control. At each load level, the displacement control is recycled thrice. With respect to the loading of the interior joints, synchronous loading of the left and right ends of the beam was performed at identical rates.

3. Results and Discussion

3.1. Cracking Patterns. Under the cyclic load, the failure process and failure pattern of the same type of specimen were essentially similar. First, the HPFRC beam-column joint specimens crack at the end of the beam under the action of bending moment, cracks then appeared in the joint region, and finally, the shear failure of the joint region occurs under repeated loads. Based on the cracking development, the failure process of the HPFRC joints was divided into three stages, namely, the elastic stage, elastic-plastic stage, and failure stage.

Table 1: Specimen parameters.

Specimen	Joint types	Beam		Column			
		Dimensions $b_b \times h_b$ (mm × mm)	Tension longitudinal bars	Dimensions $b_c \times h_c$ (mm × mm)	Reinforcing bars	Test axial compression ratio	Reinforcement in joint region
EJ-1	Exterior joints	150 × 250	3D14	200 × 200	4D14	0.10	0
EJ-2	Exterior joints	150 × 250	3D14	200 × 200	4D14	0.17	0
EJ-3	Exterior joints	150 × 250	2D14 + 1D10	200 × 200	4D14	0.10	5D6 (two legs hoop)
EJ-4	Exterior joints	150 × 250	3D14	200 × 200	4D14	0.17	1D6 (two legs hoop)
EJ-5	Exterior joints	150 × 250	3D14	200 × 200	4D14	0.10	2D6 (two legs hoop)
EJ-6	Exterior joints	150 × 250	3D14	200 × 200	4D14	0.17	2D6 (two legs hoop)
EJ-7	Exterior joints	150 × 250	3D14	200 × 200	4D14 + 2D10	0.17	0
EJ-8	Exterior joints	150 × 250	2D14 + 1D10	200 × 200	4D14	0.17	0
EJ-9	Exterior joints	150 × 250	2D20 + 1D10	200 × 200	4D14	0.11	1D6 (two legs hoop)
EJ-10	Exterior joints	150 × 250	2D20 + 1D10	200 × 200	4D14	0.18	1D6 (two legs hoop)
EJ-H1	Exterior joints	150 × 250	3D14	200 × 200	4D14	0.11	0
EJ-H2	Exterior joints	150 × 250	3D14	200 × 200	4D14	0.11	1D6 (two legs hoop)
J-1	Interior joints	250 × 350	3D14	200 × 200	4D14	0.11	0
J-2	Interior joints	250 × 350	3D14	200 × 200	4D14	0.20	0
J-3	Interior joints	250 × 350	3D14	200 × 200	4D14	0.11	1D6 (two legs hoop)
J-4	Interior joints	250 × 350	3D14	200 × 200	4D14	0.20	1D6 (two legs hoop)
LJ-1	Interior joints	250 × 350	2D22 + 1D20	300 × 300	4D22 + 4D20	0.10	0
LJ-2	Interior joints	250 × 350	2D22 + 1D20	300 × 300	4D22 + 4D20	0.10	0
LJ-3	Interior joints	250 × 350	2D22 + 1D20	300 × 300	4D22 + 4D20	0.10	1D10 (four legs hoop)
LJ-4	Interior joints	250 × 350	2D22 + 1D20	300 × 300	4D22 + 4D20	0.10	3D10 (four legs hoop)
LJ-5	Interior joints	250 × 350	2D22 + 1D20	300 × 300	4D22 + 4D20	0.10	5D10 (four legs hoop)
LJ-6	Interior joints	250 × 350	2D22 + 1D20	300 × 300	4D22 + 4D20	0.10	2D14 (web reinforcement)
LJ-7	Interior joints	250 × 350	2D22 + 1D20	300 × 300	4D22 + 4D20	0.10	4D14 (web reinforcement)
LJ-8	Interior joints	250 × 350	2D22 + 1D20	300 × 300	4D22 + 4D20	0.10	2D20 (vertical reinforcement)

In fact, the specimen was basically in the elastic phase before cracking. The strain of stirrups and HPFRC in the joint region was extremely small, and the strain essentially recovered after unloading. However, the cracks appeared at the end of the beam that was adjacent to the joint, and the cracks at the end of the beam developed slowly. The strength degradation and stiffness degradation of the joints were not obvious under repeated loading and unloading, and the residual deformation of the joint was low.

The HPFRC located in the central section of the joint region was in the state of two-way tension and compression. When the maximum tensile strain of the joint region reached the ultimate tensile strain of HPFRC, cracks were observed in the HPFRC. The first crack was typically located

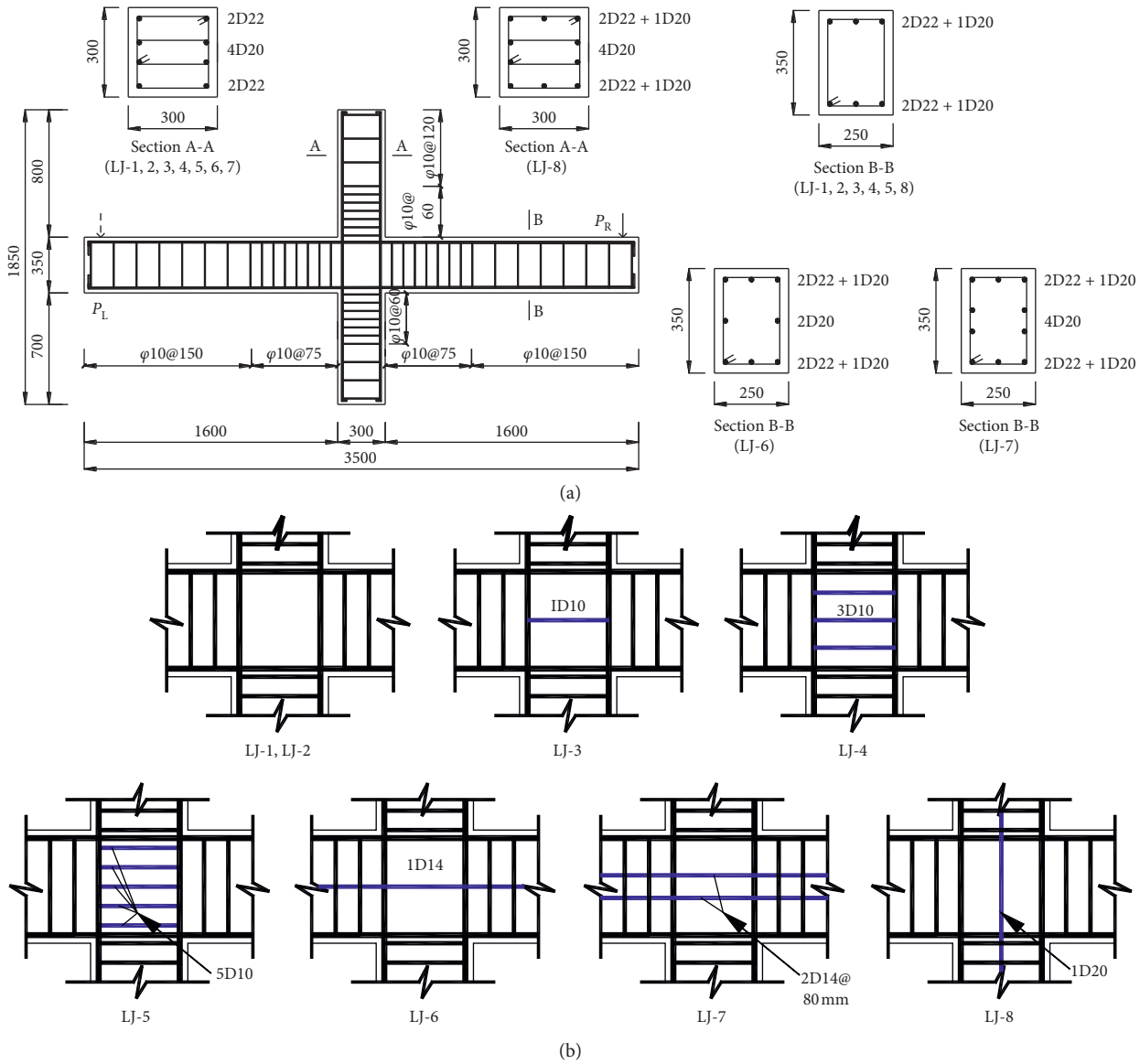

Figure 1: Details of test specimens. (a) Sizes and reinforcement of beam and column and (b) reinforcement details of joint region.

Table 2: Material parameters of reinforcement.

Reinforcement grade	Application	Diameter (mm)	Yield strength (MPa)	Ultimate strength (MPa)
600	Longitudinal bars	22	612.5	796.4
600	Longitudinal bars	20	633.3	824.9
600	Longitudinal bars	14	651.0	861.7
400	Longitudinal bars	22	455.8	625.9
400	Longitudinal bars	20	441.9	588.6
400	Longitudinal bars	14	423.4	632.4
300	Transverse stirrups	10	360.6	522.2
300	Transverse stirrups	6	353.6	398.3

near the center of the core and approximately along the diagonal direction. By reverse loading, diagonal cracks were observed on the other side of the joint region. The strain of the stirrup in the joint was low when the joint region cracked. At this phase, the stirrups played a small role, the tension stress was mainly borne by HPFRC, and the diagonal compression was completely borne by HPFRC.

With the increase of the amplitude of loading displacement and the number of cycles, several small cracks parallel to diagonal appeared in the joint, which divided the

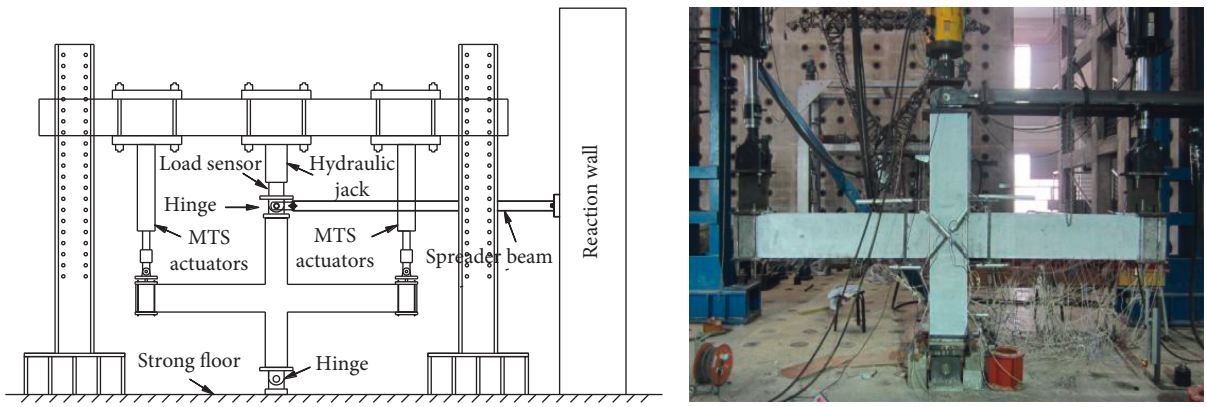

Figure 2: Test setup. (a) Schematic diagram of the test loading device and (b) field photo.

joint region into diamond blocks. The development of the main diagonal crack propagated across the entire joint area, and formed a penetrating crack, and the maximum width of the main crack was approximately 0.3~0.9 mm.

After forming a penetrating crack, diagonal cracks continued to develop with further increase in the loading displacement amplitude and this extended up and down to the column. At this moment, the width of the main crack increased significantly. A portion of the steel fiber that acts as a "bridge" at both ends of the main diagonal crack was pulled out, and a small amount of HPFRC peeling phenomenon occurred in the intersecting position of the main cracking. New cracks continued to exist on both sides of the crack and at the edge of the column although the length and width of the new crack were smaller. The strain of stirrups in the joint region increased rapidly, and when the maximum load (ultimate load) was reached, the stirrups in the joint region had yield. At this stage, the stirrups played a more significant role, the diagonal tension stress was shared by the stirrups and HPFRC, and the diagonal compression was still borne by HPFRC. As the loading displacement amplitude and cycle times continued to increase, the width of the main crack in the joint region continued to increase. The HPFRC uplift at the cross crack in the central part of the joint region was about 2~5 mm, and a small amount of HPFRC spalled along the edge of the crack.

3.2. Factors Influencing Crack Resistance of HPFRC Joints. The diagonal crack in the joint region is caused by the combined effect of tensile stress and shear stress. When the main tensile stress exceeds the ultimate tensile stress of concrete, the diagonal crack will appear. As the stress increases, the width of the crack increases. The cracking load and ultimate load of the HPFRC joint specimens are given in Table 3. The main factors affecting the cracking load and crack width of HPFRC joints include joint type, size, axial compression ratio, the stirrups ratio in joint region, the web reinforcement across the joint in beam, and the noncorner vertical reinforcement in the column.

The test results showed that, with respect to the 1/2-scale specimen, the average ratio of the cracking load to the ultimate load ranged from 0.518 to 0.704 for the exterior joint with shear failure, with a mean of 0.631. The average ratio of the cracking load to the ultimate load ranged from 0.460 to 0.604 for the interior joint with the same size, with a mean of 0.527. The average ratio of the cracking shear force of the 3/4 scale joint specimen to the peak shear force ranged from 0.271 to 0.386, with a mean of 0.318. This indicated that the cracking shear strength of the exterior joint test specimen was closer to the ultimate bearing strength. This was because of the exterior joint lateral pressure of the vertical anchoring section of the beam reinforcement to the HPFRC in the joint region was high, which could counteract the part of the tensile stress and increase the cracking strength of the exterior joint. Conversely, the inclined angle of the diagonal strut in the joint region of the exterior joint was greater than that of the specimen with the interior joint. For the exterior joint specimen, the effective area of the diagonal bar and the ultimate bearing capacity were smaller than that of the interior joint specimen. The ratio of the cracking shear force to peak shear force of the large-scale specimen was lower than that of the small-scale specimen. This can be attributed to the uneven distribution of shear stress in the HPFRC joint region. The tensile stress in central area was greater than that of others in the joint. Additionally, the peak shear force was related to the inclined compression bar and the collocation of stirrups in the joint region.

There was size effect in the cracking strength of HPFRC joints at crack. With the increase of the cross-section size of joints, the average shear stress decreased when the joints cracked. The average cracking shear stress of the interior joint specimen in 1/2 scale was 4.30 MPa while that 3/4-scale interior joint specimen was 3.01 MPa. It was evident that the average cracking shear stress of interior joint specimens in 1/2 scale was slightly higher than that of 3/4-scale specimens.

As the increase of the axial compression ratio, the cracking shear strength of HPFRC beam-column joints increased and the quantity and distribution range of cracks in the joint region of joints increased. This was owing to the area of the compression zone of the joint increased with the increase of the axial compression ratio. However, when the stirrups in the joints core decreased, the restriction of

Table 3: Test results.

Specimen	Cracking load (P_{cr} (kN))	Ultimate load (P_m (kN))	P_{cr}/P_m	Average	Specimen	Cracking load (P_{cr} (kN))	Ultimate load (P_m (kN))	P_{cr}/P_m	Average
EJ-1	+40	+59.58	0.671	0.661	J-1	+25	+49.35	0.507	0.493
	−45	−69.10	0.651			−28	−58.55	0.478	
EJ-2	+45	+53.68	0.838	0.672	J-2	+30	+57.75	0.519	0.460
	−32	−64.38	0.505			−25	−62.45	0.400	
EJ-3	+36	+45.01	0.800	0.880	J-3	+30	+52.90	0.567	0.552
	−50	−52.10	0.960			−30	−55.85	0.537	
EJ-4	+50	+58.38	0.856	0.809	J-4	+35	+51.75	0.676	0.604
	−50	−65.65	0.762			−30	−56.50	0.531	
EJ-5	+35	+52.96	0.661	0.630	LJ-1	+40	+110.61	0.362	0.386
	−40	−66.79	0.599			−40	−97.67	0.410	
EJ-6	+45	+60.05	0.749	0.763	LJ-2	+30	+123.33	0.243	0.271
	−50	−64.36	0.777			−35	−117.08	0.299	
EJ-7	+40	+56.63	0.706	0.706	LJ-3	+35	+133.34	0.262	0.275
	−45	−63.81	0.705			−40	−139.07	0.288	
EJ-8	+41	+50.80	0.807	0.758	LJ-4	+40	+109.72	0.365	0.381
	−43	−60.61	0.709			−40	−100.77	0.397	
EJ-9	+35	+63.20	0.554	0.605	LJ-5	+40	+120.15	0.333	0.332
	−50	−76.20	0.656			−40	−121.13	0.330	
EJ-10	+55	+65.55	0.839	0.697	LJ-6	+35	+134.91	0.259	0.286
	−50	−90.03	0.555			−40	−127.66	0.313	
EJ-H1	+35	+41.87	0.836	0.704	LJ-7	+40	+154.99	0.258	0.283
	−40	−69.82	0.573			−45	−146.03	0.308	
EJ-H2	+42	+75.23	0.558	0.518	LJ-8	+35	+116.63	0.300	0.328
	−44	−92.17	0.477			−40	−112.52	0.355	

stirrups to HPFRC in the joint region was insufficient, and thereby resulted in the occurrence of more small cracks. At the failure stage, with the increase of the axial compression ratio, a number of compressive cracks close to the vertical distribution were added in the upper and lower end columns of the joint region, which indicated that almost the complete cross section of the joint region is under compression.

Stirrups have a restraint effect on HPFRC in the joint region. The restraint effect of stirrups was more obvious in the joint region after the crack, which can restrain the excessive growth of crack width and reduce the crack width. Figure 3 shows the influence of the stirrup ratio on crack width of the HPFRC joint. It can be found that the crack width of specimen LJ-2 without stirrups in the joint region was always larger than that of other specimens. Especially in the failure stage, the crack width of specimen LJ-2 increased significantly. However, the crack width of the specimen with stirrups was restricted by the constraint of stirrups. With the increase of the stirrups ratio in the joint region, the spacing of stirrups decreased, the average spacing of cracks in the joint region, and the diagonal cracks width decreased, respectively. Thus, the appropriate configuration of stirrups in the joint region can reduce and restrain the development of diagonal cracks.

Figure 4 shows the influence of web reinforcement in the beam and noncorner vertical reinforcement in the column on the crack width of joints. In the early stages of diagonal cracks, the web reinforcement in the beam across the joint and noncorner vertical reinforcement in the column has little effect on the development of diagonal cracks. When the load exceeds 70% of the peak load, the crack width of LJ-1

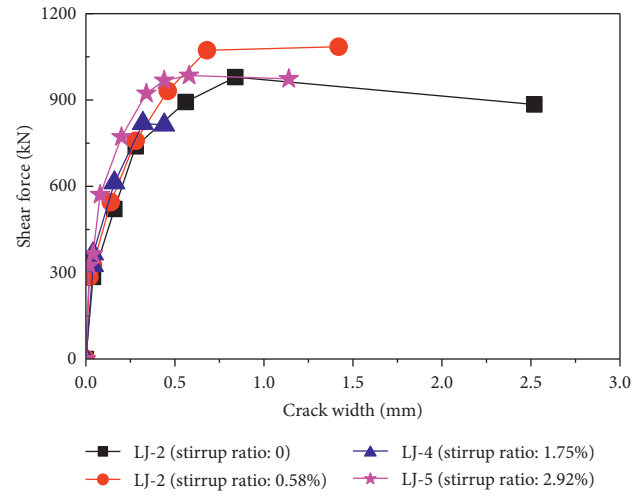

Figure 3: The influence of the stirrup ratio in the joint region on crack width.

increases rapidly, but the increase of crack width of LJ-6, LJ-7, and LJ-8 was still slow under the same load level. This is because the restraint effects of the web reinforcement and the noncorner vertical reinforcement in the column on the diagonal crack were relatively weak at the stage of the diagonal crack formation. When the diagonal crack develops to a certain extent, the shear compression area of HPFRC degenerates and the crack width and reinforcement stress increased rapidly. The bonding between the web reinforcement and HPFRC was strengthened gradually, and the dowel action of the noncorner vertical reinforcement in the column was

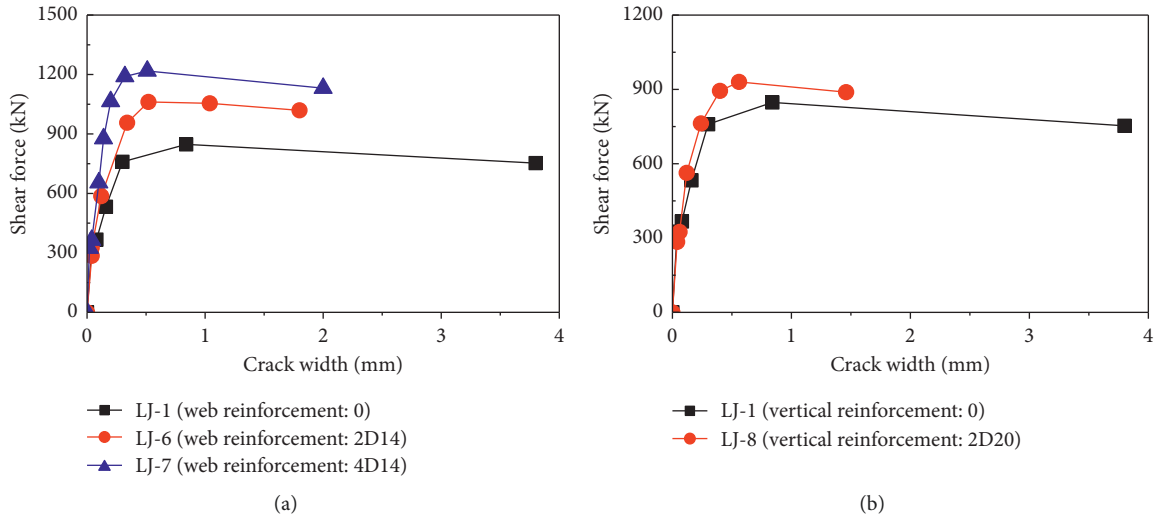

FIGURE 4: The influence of web reinforcement in the beam and noncorner vertical reinforcement in the column on the crack width of joints. The influence of (a) web reinforcement in the beam and (b) noncorner vertical reinforcement in the column.

gradually enhanced, which limited the growth rate of the diagonal crack width in the joint region. At the failure stage, the growth rate of crack width of LJ-7 was larger than that of specimen LJ-6, which may be due to the different positions of the web reinforcement. The web reinforcement of LJ-7 was located in the middle of the beam, the position was where the largest width of the diagonal cracks. At this time, the restraining effect of the web reinforcement on the diagonal crack width in the joint region was more obvious.

4. Cracking Strength of HPFRC Beam-Column Joints

4.1. Calculation for Cracking Strength. Based on the test results and multitudinous test results of normal concrete, the diagonal cracking first appeared at the center of the joint region and then extended diagonally. The joint region before the joints cracking was essential in the elastic stage [27, 28]. Thus, it was assumed that the joint region before the HPFRC joints cracked was in the elastic phase. The maximum principal tensile stress of the joints appears at the central point of the joint core. During crack, the stress of steel bars (transverse bars and column longitudinal bars) that penetrated the joint was extremely small, and the shear force of the joints was mainly undertaken by HPFRC. The crack occurred when HPFRC reaches tensile strength.

The distribution of shear stress in the joint region was uneven when the crack appear, so we introduced the inhomogeneous coefficient of shear stress distribution, namely, β_{cr}. The shear stress (τ_{cr}) of the joints at the crack was obtained as follows:

$$\tau_{cr} = \frac{V_{jcr}}{\beta_{cr} b_j h_j}, \tag{1}$$

where V_{jcr} denotes the shear force in the joint at the crack, b_j is the effective cross-section width of the joint region, and h_j is the height of the cross section of the joint region of HPFRC joints.

A tiny plane element was obtained from the central point of the HPFRC joint region for the stress analysis, and the direction of the principal stress is shown in Figure 5. On the basis of the basic theory of mechanics, the principal tensile stress σ_1 of HPFRC at the point could be obtained as follows:

$$\sigma_1 = -\frac{\sigma_c'}{2} + \sqrt{\tau_{cr}^2 + \left(\frac{\sigma_c'}{2}\right)^2}, \tag{2}$$

where σ_c' denotes the axial compressive stress of the column, $\sigma_c' = N/(b_c h_c) = n f_c$, n is the axial compressive ratio and f_c denotes the compressive strength of HPFRC.

When the crack appeared in the joint region, the principal tensile stress (σ_1) at the central point of the core was equal to the sum of the stress in the direction of the principal tensile stress of HPFRC at the point. The strain of stirrup in the joint region is small at cracking, and the tensile stress of the reinforced bar in the joint region is smaller. The sum stress in the direction of the principal tensile stress of HPFRC and the reinforcement is close to the crack tensile strength of HPFRC ($f_{t,cr}$). The crack tensile strength of HPFRC ($f_{t,cr}$) is about 87% of the tensile strength of HPFRC [29]. So, we assume that the sum stress in the direction of the principal tensile stress of HPFRC and the reinforcement is close to the tensile strength of HPFRC (f_t). This was expressed as follows:

$$-\frac{\sigma_c'}{2} + \sqrt{\tau_{cr}^2 + \left(\frac{\sigma_c'}{2}\right)^2} = f_t. \tag{3}$$

According to equation (3),

$$\tau_{cr}^2 + \left(\frac{\sigma_c'}{2}\right)^2 = \left(f_t + \frac{\sigma_c'}{2}\right)^2. \tag{4}$$

Combining (1) with (4), the shear force on the joint when it cracked was obtained as follows:

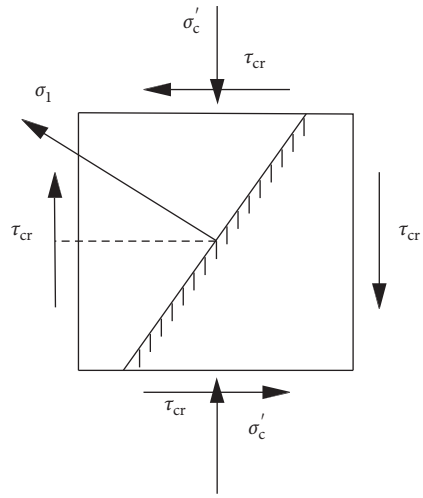

Figure 5: Center point stress of the joint core.

$$V_{jcr} = \beta_{cr} f_t b_j h_j \sqrt{1 + \frac{n f_c}{f_t}}. \quad (5)$$

In this study, a regression analysis was performed on the test results for the HPFRC tensile strength and cube compressive strength reported in previous studies [29–33], and the relation between steel fiber HPFRC tensile strength and cube compressive strength was obtained as follows:

$$f_t = 0.503 f_{cu}^{0.55}, \quad 100 \le f_{cu} \le 160, \quad (6)$$

where f_{cu} is the cube compressive strength of HPFRC, $f_c = 0.869 f_{cu}$.

Test results indicate that stirrups in the joint region have certain influences on cracking strength, and an influence coefficient (α_{cr}) of reinforcement in the joint region of the HPFRC joint is introduced to consider the effect of stirrups on the joint on cracking strength of the joint. So, the shear force of the joint at the crack can be calculated as follows:

$$V_{jcr} = \alpha_{cr} \beta_{cr} f_t b_j h_j \sqrt{1 + \frac{n f_c}{f_t}}. \quad (7)$$

We compared the test results of cracking strength with stirrups and no stirrups in the joint region. When there were stirrups in the joint region, $\alpha_{cr} = 1.06$ was recommended; otherwise, $\alpha_{cr} = 1.0$ was recommended. The inhomogeneous coefficient of the shear force distribution was obtained by the regression analysis and $\beta_{cr} = 0.58$.

4.2. Verification of the Cracking Strength Formula. Based on equation (7), the cracking strength of 24 reinforced HPFRC beam-column joints in the test was calculated. The calculated results were compared with the experimental values of the cracking strength. The results of the comparison are presented in Table 4. The average of the ratio value between the calculated value and the test results of 24 specimens was 1.030, the mean square error was 0.107, and the variable coefficient was 0.103. This illustrated that the calculated values based on the formula fit well with the experimental values.

5. Calculation for the Width of Diagonal Cracks in the Joint Region

The shear strength of the HPFRC beam-column joint is mainly borne by three parts: the diagonal strut of HPFRC, the transverse reinforcement in the joint region, and the steel fiber [34]. That is,

$$V_u = V_{RPC} + V_s + V_f. \quad (8)$$

With the increase of the load and the development of diagonal cracks, the shear resistance of steel fiber and the diagonal strut of HPFRC decrease gradually. However, the change between the two is interrelated, and it is difficult to measure them separately in the experiment. Besides considering the size effect of cracking strength and ultimate strength, $(160000/b_j h_j) K V_{jcr} = V_{RPC} + V_f$ was used to represent the shear capacity of the joints without transverse reinforcement. Hence,

$$V_u = \frac{160000}{b_j h_j} K V_{jcr} + V_s, \quad (9)$$

where K is the cracking strength coefficient of the HPFRC beam-column joint; V_{jcr} is the shear cracking load in the joint region of the HPFRC frame, which comprehensively reflects the shear force borne by HPFRC and steel fiber in the shear compression area when the joint region is cracked.

$$V_{jcr} = 0.58 f_{t,RPC} b_j h_j \sqrt{1 + \frac{n f_{c,RPC}}{f_{t,RPC}}}. \quad (10)$$

In this paper, the calculation formula of the diagonal crack was derived based on the bond-slip between steel bar and concrete. The crack width was calculated by the change of the average stress of the transverse reinforcement in the joint region. In the aspect of transferring the horizontal shear force, the effect of the web reinforcement across the joint in the beam was assumed to be the same as that of the stirrup parallel to the direction of the force, so it is equivalent to the stirrups for the analysis:

$$V_s = V_{sv} = A_{sv} \cdot \sigma_{sv,m} \cdot \frac{h_b}{s} = \rho_{sv} b_c h_b \sigma_{sv,m}. \quad (11)$$

where A_{sv} is the area of single-leg hoop and s is the stirrup spacing. Bringing formula (9) into formula (11), we get the following formula:

$$\sigma_{sv,m} = \frac{\left(V_u - \left(160000/b_j h_j\right) K V_{jcr}\right)}{\rho_{sv} b_c h_b}. \quad (12)$$

It was assumed that the stress and strain of stirrups conform to Hooke's law; that is, $\sigma_{sv} = E_{sv} \varepsilon_{sv,m}$, so

$$\varepsilon_{sv,m} = \frac{\left(V_u - \left(160000/b_j h_j\right) K V_{jcr}\right)}{E_{sv} \rho_{sv} b_c h_b}. \quad (13)$$

According to the theory of bond-slip, the width of the crack is equal to the deformation difference between steel bar and concrete in the range of crack spacing. If the vertical distance between cracks is l, then

Table 4: Comparison of HPFRC joint cracking strength between calculated values and experimental values.

Specimen	Loading direction	Experiment values (V_{jcr}^{t} (kN))	Calculated values (V_{jcr}^{c} (kN))	V_{jcr}^{c}/V_{jcr}^{t}	Specimen	Loading direction	Experiment values (V_{jcr}^{t} (kN))	Calculated values (V_{jcr}^{c} (kN))	V_{jcr}^{c}/V_{jcr}^{t}
EJ-1	Positive	139.13	144.17	0.965	J-1	Positive	156.52	162.11	0.966
	Negative	156.52	144.17	1.086		Negative	175.31	162.11	1.081
EJ-2	Positive	156.52	117.08	1.337	J-2	Positive	187.83	162.11	1.159
	Negative	113.04	117.08	0.966		Negative	156.52	162.11	0.966
EJ-3	Positive	125.22	129.75	0.965	J-3	Positive	187.83	194.54	0.965
	Negative	173.91	129.75	1.340		Negative	187.83	194.54	0.965
EJ-4	Positive	173.91	180.21	0.965	J-4	Positive	219.13	194.54	1.126
	Negative	191.30	180.21	1.062		Negative	187.83	194.54	0.965
EJ-5	Positive	121.74	126.15	0.965	LJ-1	Positive	338.79	350.89	0.966
	Negative	139.13	126.15	1.103		Negative	338.79	350.89	0.966
EJ-6	Positive	156.52	162.19	0.965	LJ-2	Positive	254.09	296.07	0.858
	Negative	173.91	162.19	1.072		Negative	296.44	296.07	1.001
EJ-7	Positive	139.13	144.17	0.965	LJ-3	Positive	296.44	307.03	0.966
	Negative	156.52	144.17	1.086		Negative	338.79	307.03	1.103
EJ-8	Positive	142.61	147.70	0.966	LJ-4	Positive	337.66	349.72	0.966
	Negative	149.57	147.70	1.013		Negative	337.66	349.72	0.966
EJ-9	Positive	121.74	126.09	0.966	LJ-5	Positive	337.66	349.72	0.966
	Negative	173.91	126.09	1.379		Negative	337.66	349.72	0.966
EJ-10	Positive	191.30	180.12	1.062	LJ-6	Positive	296.44	307.03	0.966
	Negative	173.91	180.12	0.966		Negative	338.79	307.03	1.103
EJ-H1	Positive	121.74	126.09	0.966	LJ-7	Positive	338.79	348.54	0.972
	Negative	139.13	126.09	1.103		Negative	381.14	348.54	1.094
EJ-H2	Positive	149.57	148.71	1.006	LJ-8	Positive	295.45	306.00	0.966
	Negative	156.52	148.71	1.053		Negative	337.66	306.00	1.103

$$\omega_m = \left(\int_0^l \varepsilon_{sv,x} dx - \int_0^l \varepsilon_{c,x} dx \right) \cdot \cos\theta,$$
$$\sigma_{sv,m} = \frac{1}{l_s} \int_0^l \sigma_{sv,x} dx, \tag{14}$$

where $\varepsilon_{sv,x}$ is the stirrups strain and $\varepsilon_{c,x}$ is the strain of HPFRC.

The strain of HPFRC is much smaller than that of the steel bar at the peak load, so the strain of HPFRC can be neglected. The average crack width in the joint region is obtained as follows:

$$\omega_m = \frac{\left(V_u - \left(160000/b_j h_j\right) K V_{jcr}\right)}{E_{sv}\rho_{sv} b_c h_b} l \cos\theta. \tag{15}$$

The angle of diagonal crack varies within a certain range. In the experiment, the angle of inclination is in the range of 46°~70°, and the strain of stirrups is not uniform along the length. Defining the coefficient $\phi = l \cos\theta$, the following equation is obtained:

$$\omega_m = \frac{\left(V_u - \left(160000/b_j h_j\right) K V_{jcr}\right)}{E_{sv}\rho_{sv} b_c h_b} \cdot \phi. \tag{16}$$

From formula (12), we can obtain the following formula:

$$K = \frac{\left(V_j - \sigma_{sv,m}\rho_{sv} b_c h_b\right) b_j h_j}{160000 V_{jcr}}. \tag{17}$$

By regression analysis of the relationship between shearing force V_j and parameter K, the expression of K is obtained, it is $K = 0.00159V_j$. Figure 6 is the result of linear regression.

Substituting K into formula (17), we can obtain the following formula:

$$\omega_m = \frac{\left(V_j - \left(254.4/b_j h_j\right) V_{jcr}\right)}{E_{sv} b_c h_b \rho_{sv}} \cdot \phi. \tag{18}$$

According to the cracking strength and the crack width in different loads, the expression of ϕ was obtained by regression analysis (Figure 7):

$$\phi = \frac{3112V_j - 420750}{b_j h_j}. \tag{19}$$

By combining formulas (18) and (19), we can obtain the following formula for calculating the width of diagonal cracks in the joint region:

$$\omega_m = \frac{\left(V_j - \left(254.4V_{jcr}/b_j h_j\right)\right)\left(3112V_j - 420750\right)}{E_{sv} b_c h_b \rho_{sv} b_j h_j}. \tag{20}$$

6. Conclusions

(1) Under the same cross-section condition, the cracking strength of the exterior joint was higher than that of the interior joint. The inclination angle of diagonal cracks in the exterior joint was larger than that of the

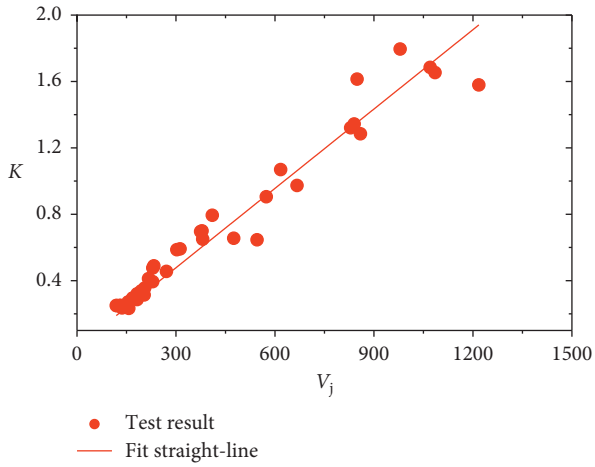

Figure 6: Regression curve of $K - V_j$.

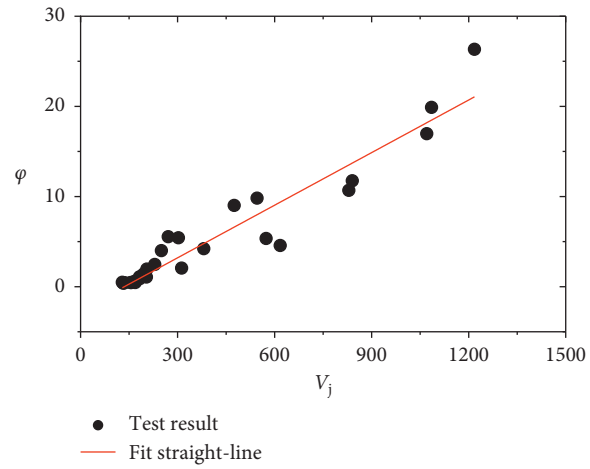

Figure 7: Regression curve of $\phi - V_j$.

interior joint, and the ultimate bearing capacity of the exterior joint was lower than that of the interior joint.

(2) A size effect of cracking strength was observed in HPFRC beam-column joints. The average shear stress at cracking decreased with the increase of the joints size.

(3) Web reinforcement and noncorner vertical reinforcement across the joint region have no evident influence on the cracking strength of the joint, but they significantly affect the distribution and width of cracks in the joint region.

(4) Based on experiment and theoretical analysis, formulas for calculating the cracking strength and crack width of HPFRC joints were proposed.

Data Availability

The experimental data of this study are included within the article. We have received permission from some researchers to quote their data to support the findings of this study that are included within the article.

Conflicts of Interest

The authors declare that they have no conflicts of interest regarding the publication of this paper.

Acknowledgments

The authors gratefully acknowledge the Natural Science Foundation of China (Grant nos. 51378095 and 51878128) and the Jilin Province Education Department "the 13th Five-Year Plan" Science and Technology Research Project (Project no. JJKH20190695KJ).

References

[1] C. Q. Li and R. E. Melchers, "Analytical model for corrosion-induced crack width in reinforced concrete structures," *ACI Structural Journal*, vol. 103, no. 4, pp. 479–487, 2006.

[2] K. Yamamoto, T. Isoda, and T. Saito, "A study of reinforced concrete structures deterioration in coastal area by focusing on condition of bar corrosion," *Journal of Japan Society of Civil Engineers, Ser. B3 (Ocean Engineering)*, vol. 72, no. 2, pp. I_604–I_609, 2016.

[3] F. Cao, H. Zhou, and L. L. Shuangying, "Analysis on durability and lifting technology improvement of concrete in Qinghai salt lake area," *Low Temperature Architecture Technology*, vol. 39, no. 11, pp. 4–6, 2017.

[4] B. H. Oh and Y. J. Kang, "New formulas for maximum crack width and crack spacing in reinforced concrete flexural members," *ACI Structural Journal*, vol. 84, no. 2, pp. 103–112, 1987.

[5] L. Biolzi and S. Cattaneo, "Response of steel fiber reinforced high strength concrete beams: experiments and code predictions," *Cement and Concrete Composites*, vol. 77, pp. 1–13, 2017.

[6] S. D. Silva, H. Mutsuyoshi, and E. Witchukreangkrai, "Evaluation of shear crack width in I-shaped prestressed reinforced concrete beams," *Journal of Advanced Concrete Technology*, vol. 6, no. 3, pp. 443–458, 2008.

[7] A. Muttoni and M. F. Ruiz, "Shear strength of members without transverse reinforcement as function of critical shear crack width," *ACI Structural Journal*, vol. 105, no. 2, pp. 163–172, 2008.

[8] M. A. Mansur, K. H. Tan, and S. L. Lee, "Crack width in concrete members reinforced with welded wire fabric," *ACI Structural Journal*, vol. 88, no. 2, pp. 147–154, 1991.

[9] G. H. Xing, T. Wu, and B. Q. Liu, "Study on crack resistance of beam-column joints in reinforced concrete frame structures," *Engineering Mechanics*, vol. 28, no. 3, pp. 163–169, 2011.

[10] A. Filiatrault, S. Pineau, and J. Houde, "Seismic behavior of steel-fiber reinforced concrete interior beam-column joints," *ACI Material Journal*, vol. 92, no. 5, pp. 543–552, 1995.

[11] R. Yu, P. piesz, and H. J. H. Brouwers, "Development of an eco-friendly ultra-high performance concrete (UHPC) with efficient cement and mineral admixtures uses," *Cement & Concrete Composites*, vol. 55, no. 1, pp. 383–394, 2017.

[12] V. Afroughsabet, L. Biolzi, and T. Ozbakkaloglu, "High-performance fiber-reinforced concrete: a review," *Journal of Materials Science*, vol. 51, no. 14, pp. 6517–6551, 2016.

[13] J.-G. Choi, G.-C. Lee, and K.-T. Koh, "The effects of mixture rate and aspect ratio of steel fiber on mechanical properties of ultra high performance concrete," *Journal of the Korean*

Recycled Construction Resources Institute, vol. 5, no. 1, pp. 14–20, 2017.

[14] A. Mo, S. El-Tawil, Z. Liu, and W. Hansen, "Effects of silica powder and cement type on durability of ultra high performance concrete (UHPC)," *Cement & Concrete Composites*, vol. 66, pp. 47–56, 2016.

[15] M. Singh, A. H. Sheikh, M. S. Mohamed Ali, P. Visintin, and M. C. Griffith, "Experimental and numerical study of the flexural behaviour of ultra-high performance fibre reinforced concrete beams," *Construction and Building Materials*, vol. 138, pp. 12–25, 2017.

[16] D.-Y. Yoo, N. Banthia, and Y.-S. Yoon, "Flexural behavior of ultra-high-performance fiber-reinforced concrete beams reinforced with GFRP and steel rebars," *Engineering Structures*, vol. 111, pp. 246–262, 2016.

[17] W. Zhou, H. Hu, and W. Zheng, "Bearing capacity of reactive powder concrete reinforced by steel fibers," *Construction and Building Materials*, vol. 48, pp. 1179–1186, 2013.

[18] M. A. Al-Osta, M. N. Isa, M. H. Baluch, and M. K. Rahman, "Flexural behavior of reinforced concrete beams strengthened with ultra-high performance fiber reinforced concrete," *Construction and Building Materials*, vol. 134, pp. 279–296, 2017.

[19] W. Zheng, L. Li, and S. Lu, "Experimental research on mechanical performance of normal section of reinforced reactive powder concrete beam," *Journal of Building Structures*, vol. 32, pp. 25–134, 2011.

[20] M. Shafieifar, M. Farzad, and A. Azizinamini, "Experimental and numerical study on mechanical properties of ultra high performance concrete (UHPC)," *Construction and Building Materials*, vol. 156, pp. 402–411, 2017.

[21] T. Makita and E. Brühwiler, "Tensile fatigue behaviour of ultra-high performance fibre reinforced concrete (UHPFRC)," *Materials and Structures*, vol. 47, no. 3, pp. 475–491, 2013.

[22] S. H. Park, D. J. Kim, G. S. Ryu, and K. T. Koh, "Tensile behavior of ultra high performance hybrid fiber reinforced concrete," *Cement and Concrete Composites*, vol. 34, no. 2, pp. 172–184, 2012.

[23] W. Zheng, D. Wang, and Y. Ju, "Performance of reinforced reactive powder concrete beam-column joints under cyclic loads," *Advances in Civil Engineering*, vol. 2018, Article ID 3914815, 12 pages, 2018.

[24] D. H. Wang, Y. Z. Ju, and W. Z. Zheng, "Strength of reactive powder concrete beam-column joints reinforced with high-strength (HRB600) bars under seismic loading," *Strength of Materials*, vol. 49, no. 1, pp. 139–151, 2017.

[25] Y. Z. Ju, D. H. Wang, and M. X. Kang, "Mechanical properties of RPC with different steel fiber contents," *Journal of Basic Science & Engineering*, vol. 21, no. 2, pp. 299–306, 2013, in Chinese.

[26] JGJ 101-2015, *Specificating of Testing Methods for Earthquake Resistant Building*, China Building Industry Press, Beijing, China, 2015, in Chinese.

[27] F. Faleschini, L. Hofer, M. A. Zanini, M. dalla Benetta, and C. Pellegrino, "Experimental behavior of beam-column joints made with EAF concrete under cyclic loading," *Engineering Structures*, vol. 139, pp. 81–95, 2017.

[28] S. H. Said and H. Abdul Razak, "Structural behavior of RC engineered cementitious composite (ECC) exterior beam-column joints under reversed cyclic loading," *Construction and Building Materials*, vol. 107, pp. 226–234, 2016.

[29] L. Li, *Mechanical Behavior and Design Method for Reactive Powder Concrete Beam*, Harbin Institute of Technology, Harbin, China, 2010, in Chinese.

[30] Z. Z. Yang, *Study on Tension Mechanical Performance of Reactive Powder Concrete in Different Steel Fiber Volume Fractions*, Beijing Jiaotong University, Beijing, China, 2006, in Chinese.

[31] S. Yan, *The Research on the Tensile Performance of the Ultra-High-Performance Concrete Reinforced by grading-Fiber*, Hunan University, College of Civil Engineering, Changsha, China, 2006, in Chinese.

[32] H. Y. Yuan, A. N. Ming Zhe, F. F. Jia, and Y. U. Zi Ruo, "Experimental research on uniaxial tensile performance of reactive powder concrete," *Engineering Mechanics*, vol. 28, no. 1, pp. 141–144, 2011, in Chinese.

[33] Y. Yong, *Damage Constitutive Model of RPC under Uniaxial Tension and Compression Based on Weibull Distribution*, Jilin: Northeast Dianli University, School of Civil Engineering and Architecture, Changchun, China, 2015, in Chinese.

[34] D. Wang, Y. Ju, W. Zheng, and H. Shen, "Seismic behavior and shear bearing capacity of ultra-high performance fiber-reinforced concrete (UHPFRC) beam-column joints," *Applied Sciences*, vol. 8, no. 5, p. 810, 2018.